TGF- Signaling Is Associated with Endocytosis at the Pocket Region of the Primary Cilium

Clement, Christian Alexandro; Ajbro, Katrine Dalsgaard; Koefoed, Karen; Vestergaard, Maj Linea; Veland, Iben Rønn; Perestrello Ramos H de Jesus, Maria; Pedersen, Lotte Bang; Benmerah, Alexandre; Andersen, Claus Yding; Larsen, Lars Allan; Christensen, Søren Tvorup

Published in:
Cell Reports

DOI:
10.1016/j.celrep.2013.05.020

Publication date:
2013

Document version
Publisher's PDF, also known as Version of record

Cell Reports
Report

TGF-β Signaling Is Associated with Endocytosis at the Pocket Region of the Primary Cilium

Christian Alexandro Clement,[1] Katrine Dalsgaard Ajbro,[2] Karen Koefoed,[1] Maj Linea Vestergaard,[1,2,3] Iben Rønn Veland,[1] Maria Perestrello Ramos Henriques de Jesus,[1] Lotte Bang Pedersen,[1] Alexandre Benmerah,[4,5] Claus Yding Andersen,[3] Lars Allan Larsen,[2,*] and Søren Tvorup Christensen[1,*]

[1]Department of Biology
[2]Wilhelm Johannsen Centre for Functional Genome Research, Department of Cellular and Molecular Medicine
[3]Laboratory of Reproductive Biology
University of Copenhagen, DK-1165 Copenhagen, Denmark
[4]INSERM, U983, Hôpital Necker-Enfants Malades, 75015 Paris, France
[5]Université Paris-Descartes, Sorbonne Paris Cité, Institut Imagine, 75015 Paris, France
*Correspondence: larsal@sund.ku.dk (L.A.L.), stchristensen@bio.ku.dk (S.T.C.)
http://dx.doi.org/10.1016/j.celrep.2013.05.020

SUMMARY

Transforming growth factor β (TGF-β) signaling is regulated by clathrin-dependent endocytosis (CDE) for the control of cellular processes during development and in tissue homeostasis. The primary cilium coordinates several signaling pathways, and the pocket surrounding the base and proximal part of the cilium is a site for CDE. We report here that TGF-β receptors localize to the ciliary tip and endocytic vesicles at the ciliary base in fibroblasts and that TGF-β stimulation increases receptor localization and activation of SMAD2/3 and ERK1/2 at the ciliary base. Inhibition of CDE reduced TGF-β-mediated signaling at the cilium, and TGF-β signaling and CDE activity are reduced at stunted primary cilia in *Tg737*^{orpk} fibroblasts. Similarly, TGF-β signaling during cardiomyogenesis correlated with accumulation of TGF-β receptors and activation of SMAD2/3 at the ciliary base. Our results indicate that the primary cilium regulates TGF-β signaling and that the ciliary pocket is a compartment for CDE-dependent regulation of signal transduction.

INTRODUCTION

Transforming growth factor β (TGF-β)/bone morphogenic protein (BMP) signaling plays critical roles in cell-cycle control, migration, differentiation, and other cellular processes throughout life (Guo and Wang, 2009). TGF-β signaling proceeds via formation of a heterotetrameric receptor complex of type I and II TGF-β receptors (TGF-β-RI and TGF-β-RII) whose activation leads to phosphorylation and activation of downstream effectors, including MEK1/2-ERK1/2 and receptor SMADs, SMAD2/3 (Huang and Chen, 2012). SMAD2/3 associates with SMAD4 in heterotrimeric complexes that translocate to the nucleus and regulate gene expression. Several feedback systems are activated upon TGF-β signaling, including SMAD7, which negatively regulates the pathway through receptor complex degradation. Internalization of TGF-β receptors (TGF-β-Rs) via clathrin-dependent endocytosis (CDE) enhances TGF-β signaling by formation of clathrin-coated vesicles (CCVs) and early endosomes (EEs) enriched in phosphatidylinositol-3 phosphate [PI(3)P]. PI(3)P anchors FYVE zinc finger domain-containing proteins, such as SMAD anchor for receptor activation (SARA) that conveys SMAD2/3 to the TGF-β-Rs and promotes TGF-β-RI-mediated SMAD2/3 activation (Tang et al., 2010; Huang and Chen, 2012).

Primary cilia coordinate multiple signaling pathways, such as receptor tyrosine kinase (RTK), Hedgehog (Hh), Wnt, Notch, and mTOR (Goetz and Anderson, 2010; Boehlke et al., 2010; Satir et al., 2010; Ezratty et al., 2011; Lienkamp et al., 2012; Christensen et al., 2012). Thus, defective primary cilia lead to aberrant cell signaling, in turn causing a series of diseases known as ciliopathies (Hildebrandt et al., 2011; Waters and Beales, 2011). We previously reported that embryos of *Tg737*/*Ift88* null mice, which have defects in the formation of primary cilia, have cardiac anomalies (Clement et al., 2009a) characteristic of aberrant TGF-β signaling (Arthur and Bamforth, 2011). Further, in *Tg737* mutant embryonic hearts, endothelial cells have altered SMAD2 phosphorylation and expression of α-smooth muscle actin (Egorova et al., 2011). Yet, a direct role for the primary cilium in coordinating TGF-β signaling is unknown.

In many cell types, the proximal part of the primary cilium resides in the cytoplasm within an invagination of the plasma membrane known as the ciliary pocket (CiPo), which is a unique domain for CDE (Poole et al., 1985; Rattner et al., 2010; Molla-Herman et al., 2010; Ghossoub et al., 2011), whose function is poorly understood. Here, we show that TGF-β signaling is associated with the CiPo region in fibroblasts and in stem cells during cardiomyocyte differentiation and identify the CiPo as a site of CDE-dependent activation of signal transduction.

RESULTS

TGF-β Induces Accumulation and Activation of TGF-β Signaling Components at the Primary Cilium in a CDE-Dependent Manner

The role of primary cilia in TGF-β signaling was first analyzed using cultures of growth-arrested fibroblasts. In human foreskin

fibroblasts (hFFs), TGF-β1 stimulation led to activation of SMAD2/3 and MEK1/2-ERK1/2 (Figures 1A–1C). Immunofluorescence microscopy (IFM) showed that TGF-β-RI and TGF-β-RII localized to the base of the primary cilium (CiBa) and sometimes to the ciliary tip in unstimulated cells. Upon 30 min of TGF-β1 stimulation, receptor localization increased at the CiBa (Figures 1D–1F) along with reduced ciliary tip localization. Occasionally, we observed receptor localization to the tip after 180 min of stimulation (Figure 1G), suggesting that activation of TGF-β signaling is associated with trafficking of receptors within the cilium and targeting to the CiBa. SMAD4 localized to the CiBa (Figure 1H) and TGF-β1 induced the phosphorylation of SMAD2/3 (p-SMAD2/3) and ERK1/2 (Figures 1I–1K and S1A) at CiBa, followed by nuclear translocation of SMAD4 and p-SMAD2/3 after 90 min of stimulation (Figures S1A and S1B). These results show that TGF-β signaling takes place at the cilium and that onset of signal transduction partly occurs at the CiBa followed by translocation of SMADs to the nucleus. We also detected SMAD7 at the CiBa (Figure 1H), indicating that deactivation of TGF-β signaling also occurs at the cilium.

To assess the role of CDE in TGF-β signaling at the cilium, hFFs were stimulated with TGF-β1 with and without Dynasore, which blocks the budding of clathrin-coated pits (CCPs) and CCV formation (Kirchhausen et al., 2008) and inhibits CDE at the CiPo region without reducing cilia formation (Molla-Herman et al., 2010). Dynasore inhibited TGF-β1-induced SMAD2/3 phosphorylation (Figures 1L and 1M) at the CiBa (Figure 1N and 1P) as well as nuclear localization of p-SMAD2/3 and SMAD4 after 90 min of TGF-β1 stimulation (Figures S1C and S1D). These results suggest that TGF-β signaling and activation of SMADs are associated with CDE at the CiBa. In contrast, activation of ERK1/2 was largely unaffected by Dynasore (Figures 1L, 1M, 1O, and 1P), indicating that this pathway is independent of CDE.

Tg737^{orpk} Fibroblasts Have Reduced TGF-β Signaling and Decreased Activity of CDE at the Ciliary Base

The importance of the primary cilium in TGF-β signaling via SMADs was tested using hypomorphic *Tg737*^{orpk} mutant mouse embryonic fibroblasts (MEFs) with stunted cilia (Schneider et al., 2005; Corbit et al., 2008). Compared to wild-type (WT) MEFs, p-SMAD2/3 levels were reduced in *Tg737*^{orpk} MEFs after TGF-β1 stimulation (Figures 2A and 2B). *Tg737*^{orpk} and WT MEFs expressed similar levels of TGF-β-RI and TGF-β-RII (Figure 2A), indicating that reduced TGF-β signaling in mutant MEFs is not due to altered receptor expression. However, upon 30 min of TGF-β1 stimulation, there was significantly less TGF-β-RI (Figure 2C) and p-SMAD2/3 (Figure 2D) at the base of stunted cilia in *Tg737*^{orpk} MEFs compared to normal cilia in WT MEFs. This was associated with reduced nuclear translocation of p-SMAD2/3 and SMAD4 after 60 min of TGF-β1 stimulation (Figure S2A–S2D). Next, cells were cultured with Texas red transferrin (TR-Tf) for 10 min to visualize CCVs and EEs (Molla-Herman et al., 2010) (Figure S2E). In WT MEFs, TR-Tf localized as multiple puncta in the cytosol and around the primary cilium as reported for other cell types (Molla-Herman et al., 2010). In contrast, TR-Tf accumulation appeared less abundant at stunted cilia in *Tg737*^{orpk} MEFs, whereas the cytosolic labeling was similar to that of WT cells. Localization of clathrin assembly lymphoid myeloid leukemia (CALM)-positive puncta was also reduced around stunted cilia in *Tg737*^{orpk} MEFs (Figure 2E). IFM and isosurface three-dimensional (3D) visualization showed that CALM localized around the proximal part and base of WT primary cilia, and this localization was reduced in *Tg737*^{orpk} MEFs (Figure 2F). Multiple CALM-positive puncta at the CiPo of WT cilia colocalized with clathrin (Figure S2F) and with TGF-β-RI (Figure 2G), indicating that TGF-β signaling is associated with CDE at the CiPo and that this is disrupted in *Tg737*^{orpk} MEFs.

TGF-β Signaling Is Upregulated during Cardiomyocyte Differentiation

TGF-β signaling plays a critical role in heart development (Arthur and Bamforth, 2011). To test whether it is associated with primary cilia during cardiomyogenesis, transcriptome analysis was performed on P19.CL6 cells during DMSO-induced cardiomyocyte differentiation (Habara-Ohkubo, 1996). Differentiation was evidenced by decreased nuclear localization of the stem cell marker SOX2 and increased nuclear localization of the cardiomyocyte transcription factor GATA4 as well as α-actinin localization to Z-lines of cardiac muscle cells at day 14 (Figure 3A). Primary cilia were formed at all stages of differentiation (Figure 3A) (Clement et al., 2009a). Transcriptome analysis revealed that several signaling pathways are affected during cardiomyogenesis, including TGFβ/BMP and Hh signaling (Figure 3B). Expression of cardiomyocyte markers and multiple TGF-β/BMP signaling components were upregulated during cardiomyogenesis (Figure 3C). Quantitative RT-PCR analysis (Figure 3D) confirmed these results. Expression of *TGF-β-RI*, *SMAD2*, *SMAD3*, and *SMAD4* all increased during differentiation in a bell-shaped fashion, peaking at day 7. *TGF-β-RII* expression increased in a more linear fashion up to day 12. In contrast, SMAD7 was downregulated during the first few days, suggesting that SMAD7-dependent inhibition of TGF-β signaling is kept low during the initial stages of differentiation. At day 12, expression levels of *TGF-β-RI*, *SMAD2*, *SMAD3*, and *SMAD4* decreased, indicative of decreased TGF-β signaling at the end stage of differentiation. Western blot (WB) analysis confirmed that the TGF-β-RI level peaks at day 7 of differentiation (Figures 3E and 3F).

TGF-β Signaling Is Associated with CDE at the Ciliary Base during Cardiomyocyte Differentiation

Next, the localization of TGF-β-RI and p-SMAD2/3 during P19.CL6 differentiation at day 1 and 7 was analyzed. TGF-β-RI accumulated around the CiBa during differentiation, along with increased SMAD2/3 activation (Figures 4A–4C). Specificity of the TGF-β-RI antibody was confirmed by peptide competition assays (Figure 4D). Similar experiments were performed with hESC (Figure S3A), which as embryoid bodies (EBs) were induced to differentiate into cardiomyocytes expressing increased levels of GATA4 and NKX2-5 (Figures S3B and S3C). At day 20 of differentiation, TGF-β-RI and p-SMAD2/3 accumulated at the hESC CiBa (Figures S3D and S3E). IFM and 3D isomeric reconstruction showed that ciliary TGF-β-RI localization is largely confined to the area surrounding the CiBa and proximal part of the cilium (Figures 4E and 4F). This region

Cell PRESS
Open ACCESS

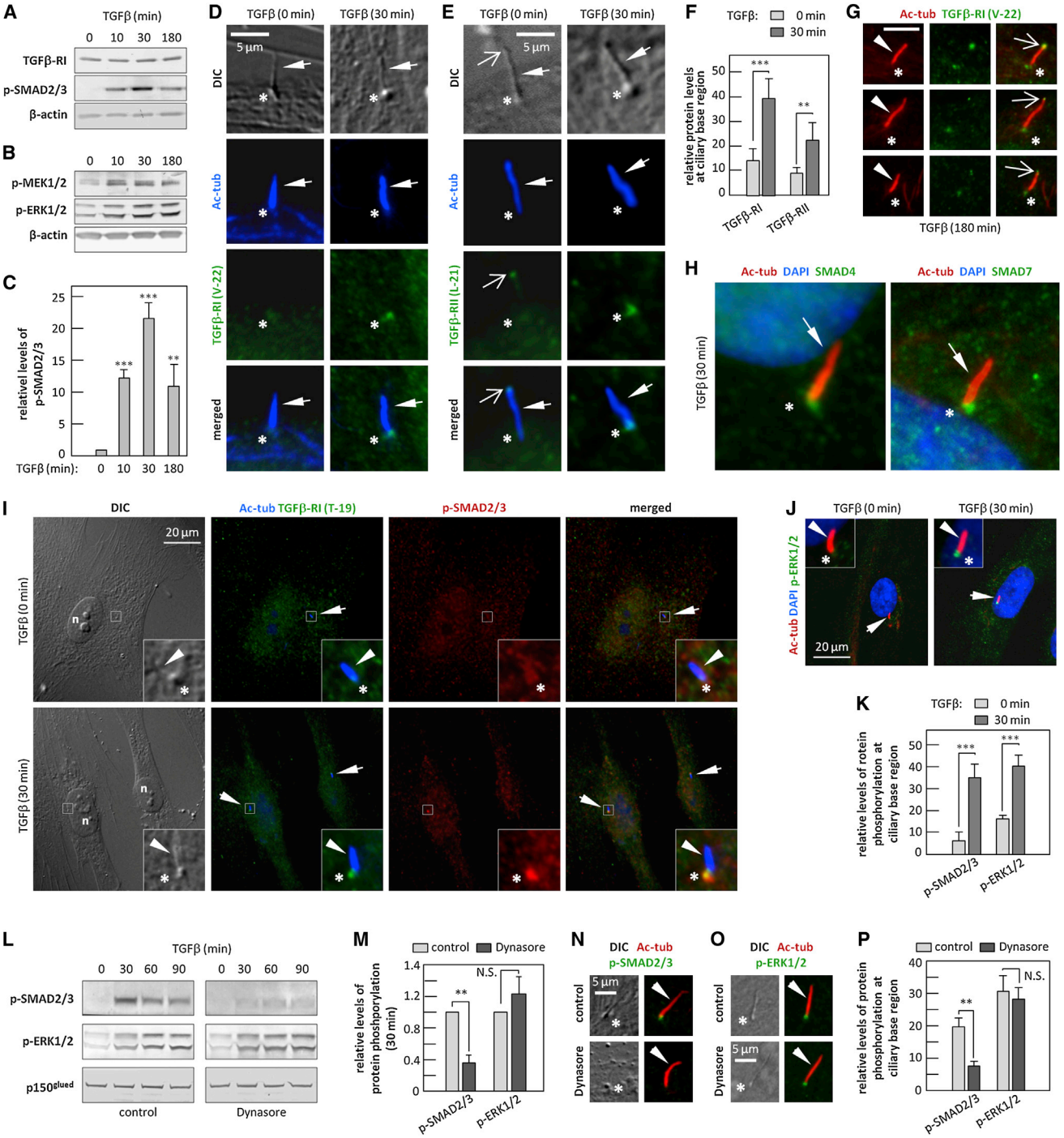

Figure 1. TGF-β Signaling at the CiBa in Growth-Arrested hFF Cells

(A and B) WB of cells treated with TGF-β1 (2 ng/ml) for 0, 10, 30, and 180 min using antibodies as indicated.

(C) Quantification of p-SMAD2/3 levels in (A) relative to 0 min. Shown are means ± SD (n = 5). **p < 0.01; ***p < 0.001.

(D and E) DIC and IFM of cells treated with TGF-β1 for 0 and 30 min, (D) anti-acetylated α-tubulin (Ac-tub), anti-TGF-β-RI(V-22), (E) anti-Ac-tub, and anti-TGF-β-RII(L-21). Bold arrows indicate primary cilia. Asterisks indicate CiBa. Open arrows indicate the ciliary tip.

(F) Quantification of TGF-β-RI and TGF-β-RII fluorescence levels at the CiBa region seen in (D) and (E). Shown are means ± SD (n = 24). **p < 0.01; ***p < 0.001.

(G) IFM of TGF-β-RI localization to the ciliary tip in cells with TGF-β1 for 180 min, anti-TGF-β-RI(V-22), and anti-Ac-tub. Bold arrows indicate primary cilia. Asterisks indicate CiBa. Open arrows indicate the ciliary tip.

(H) IFM of cells with TGF-β1 for 30 min, anti-Ac-tub and anti-SMAD4, anti-SMAD7, and DAPI. Bold arrows indicate primary cilia. Asterisks indicate CiBa.

(legend continued on next page)

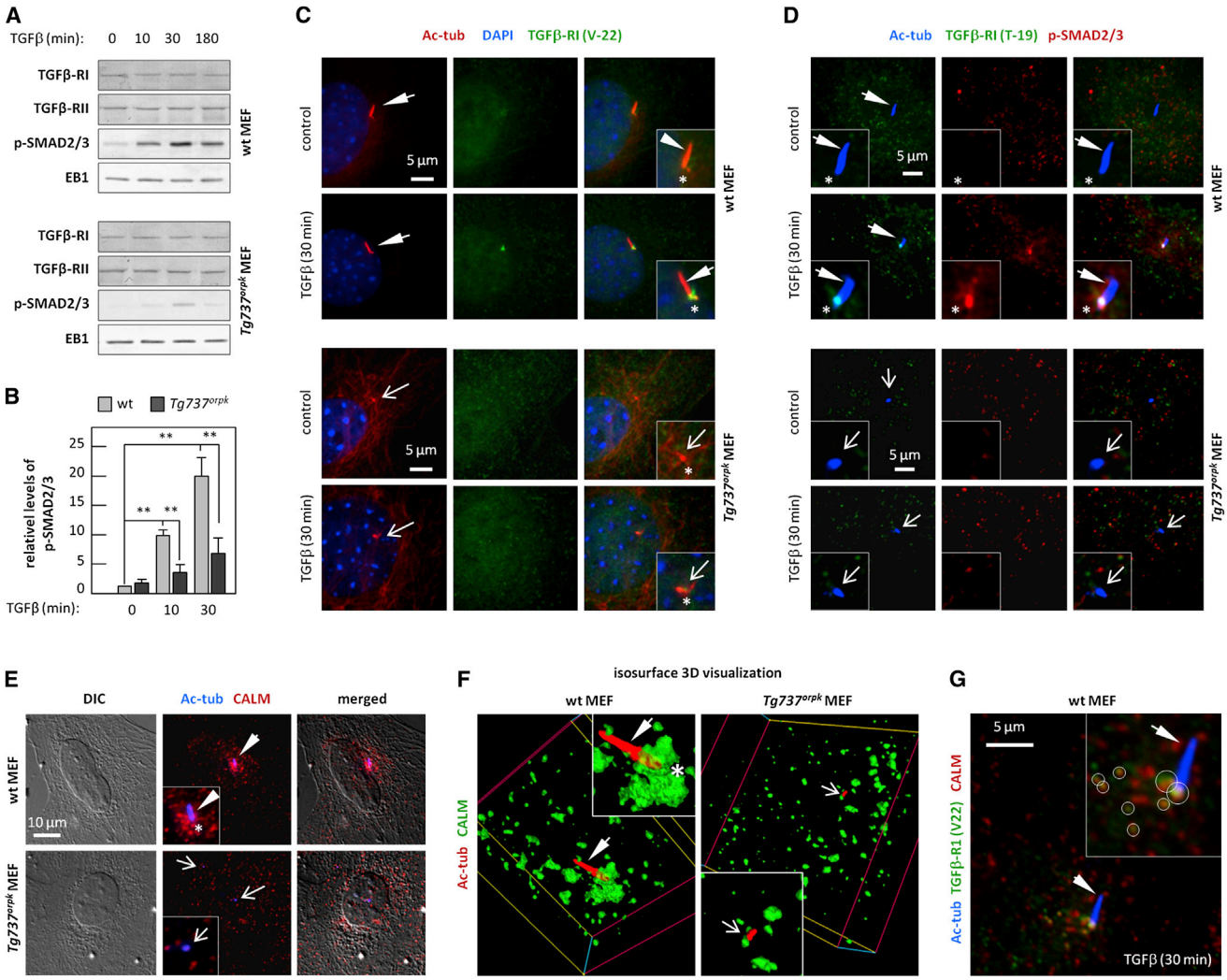

Figure 2. TGF-β Signaling and CDE Are Reduced at Stunted Primary Cilia in Growth-Arrested *Tg737*^{orpk} MEFs

(A) WB of WT and *Tg737*^{orpk} MEFs with TGF-β1 (2 ng/ml) for 0, 10, 30, and 180 min using antibodies as indicated.

(B) Quantification of p-SMAD2/3 levels with TGF-β1 for 0, 10, and 30 min as seen in (A). Shown are means ± SD (n = 5). **p < 0.01.

(C and D) IFM of WT (C) and *Tg737*^{orpk} (D) MEFs with TGF-β1 for 0 and 30 min. Bold arrows indicate primary cilia. Open arrows indicate stunted cilia. Asterisks indicate CiBa.

(E) DIC and IFM of WT and *Tg737*^{orpk} MEFs. Bold arrows indicate primary cilia. Open arrows indicate stunted cilia. Asterisks indicate CiBa.

(F) IFM with 3D reconstruction and isosurface visualization of WT and *Tg737*^{orpk} MEFs. Bold arrows indicate primary cilia. Open arrows indicate stunted cilia. Asterisks indicate CiBa.

(G) IFM of wt MEFs with TGFβ-1 for 30 min. Bold arrows indicate primary cilia. Circles indicate colocalization between TGF-β-RI and CALM.

comprises the CiPo, suggesting that TGF-β signaling takes places through CDE at this site during cardiomyocyte differentiation.

We analyzed the expression of cardiac marker proteins in P19.CL6 cells cultured in the presence of DMSO and various concentrations of TGF-β1. TGF-β1 stimulation increased the

(I and J) IFM of cells with TGF-β1 for 0 and 30 min, (I) anti-Ac-tub, anti-p-SMAD2/3, anti-TGF-β-RI(T-19), (J) anti-Ac-tub, anti-p-ERK1/2, and DAPI. Bold arrows indicate primary cilia. Asterisks indicate CiBa.

(K) Quantification of p-SMAD2/3 and p-ERK1/2 fluorescence levels at the CiBa region as seen in (I) and (J). Shown are means ± SD (n = 25). ***p < 0.001.

(L) WB of cells treated with TGF-β1 for 0, 30, and 180 min with and without Dynasore (75 μM) using antibodies as indicated.

(M) Quantification of p-SMAD2/3 and p-ERK1/2 levels in Dynasore-treated cells compared to untreated cells with TGF-β1 for 30 min as seen in (L). Shown are means ± SD (n = 5). ***p < 0.001. NS, not significant.

(N and O) DIC and IFM of cells with TGF-β1 for 30 min with and without Dynasore (75 μM). Bold arrows indicate primary cilia. Asterisks indicate CiBa.

(P) Quantification of p-SMAD2/3 and p-ERK1/2 fluorescence levels at the CiBa as seen in (N) and (O). Shown are means ± SD (n = 25). **p < 0.01. NS, not significant.

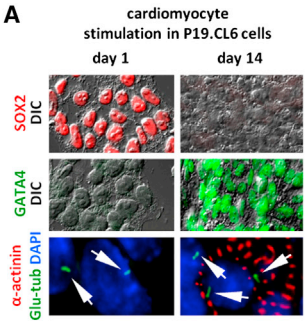

B

transcriptomics: Affected signal transduction pathways during cardiomyocyte differentiation in P19.CL6 cells from day 1 to 14 ($p<0.05$)

Signaling Pathway	DEGs with pathway annotation	All genes with pathway annotation	p-value	Pathway ID
MAPK	58 (3.53%)	267 (2.47%)	0.003	ko04010
Wnt	36 (2.19%)	154 (1.42%)	0.005	ko04310
TGFβ/BMP	19 (1.16%)	83 (0.77%)	0.040	ko04350
Hedgehog	16 (0.97%)	54 (0.5%)	0.005	ko04340
VEGF	17 (1.03%)	73 (0.67%)	0.044	ko04370
Notch	15 (0.91%)	51 (0.47%)	0.007	ko04330

C

transcriptomics: up- and down-regulation of genes during cardiomyocyte differentiation relative to day 1 (p-values in parentheses)

cardiomyocyte differentiation	transcript ID	log2 ratio (day4/day1)	log2 ratio (day7/day1)	log2 ratio (day14/day1)
Gata4	gi|110681730|ref|NM_008092.3|	N.A.	8.42 (0.101)	10.6 (0.000)
Tnni1	gi|162951866|ref|NM_001112702.1|	N.A.	9.12 (0.000)	12.6 (0.000)
Nkx2-5	gi|76677926|ref|NM_008700.2|	N.A.	N.A.	5.25 (0.001)
Myh7	gi|118131045|ref|NM_080728.2|	N.A.	N.A.	12.4 (0.000)
Alcam	gi|158937321|ref|NM_009655.2|	N.A.	N.A.	4.29 (0.003)
Id2	gi|162287136|ref|NM_010496.3|	1.91 (0.000)	2.95 (0.000)	4.06 (0.000)
Id1	gi|118130032|ref|NM_010495.2|	N.A.	1.52 (0.000)	2.12 (0.000)
Id3	gi|118130594|ref|NM_019689.2|	N.A.	N.A.	1.54 (0.000)

TGFβ/BMP signalling	transcript ID	log2 ratio (day4/day1)	log2 ratio (day7/day1)	log2 ratio (day14/day1)
TGFβ1	gi|6755774|ref|NM_011577.1|	2.33 (0.000)	2.07 (0.000)	N.A.
Bmp2	gi|71896668|ref|NM_007553.2|	5.45 (0.001)	6.72 (0.000)	6.32 (0.000)
Noggin	gi|158187522|ref|NM_008711.2|	N.A.	5.09 (0.000)	4.94 (0.000)
Lefty1	gi|126012509|ref|NM_010094.3|	1.66 (0.000)	N.A.	1.50 (0.000)
Nodal	gi|218156276|ref|NM_013611.4|	N.A.	-1.20 (0.000)	-3.22 (0.000)
TGFβ-RI	gi|40254607|ref|NM_009370.2|	N.A.	N.A.	1.57 (0.000)
TGFβ-RII	gi|239787883|ref|NM_029575.3|	N.A.	N.A.	2.44 (3.644)
TGFβ-RIII	gi|229577251|ref|NM_011578.3|	-1.70 (0.000)	-2.09 (0.000)	-1.14 (0.007)
Acv-R2a	gi|160358784|ref|NM_007396.4|	N.A.	1.53 (0.000)	1.40 (0.000)
Bambi	gi|118129835|ref|NM_026505.2|	1.72 (0.000)	2.20 (0.000)	3.05 (0.000)
Smad3	gi|254675248|ref|NM_016769.4|	N.A.	1.57 (0.000)	1.48 (0.000)
Smad6	gi|254675284|ref|NM_008542.3|	1.40 (0.000)	1.57 (0.000)	2.97 (0.000)
Smad9	gi|141802048|ref|NM_019483.4|	N.A.	N.A.	8.73 (0.004)
TGFβ-Rap1	gi|68299761|ref|NM_001013025.2|	N.A.	N.A.	2.03 (0.008)
Tab2	gi|226423910|ref|NM_138667.3|	N.A.	N.A.	1.15 (0.000)
Tgfβ1i1	gi|40254611|ref|NM_009365.2|	N.A.	2.29 (0.000)	2.39 (0.000)

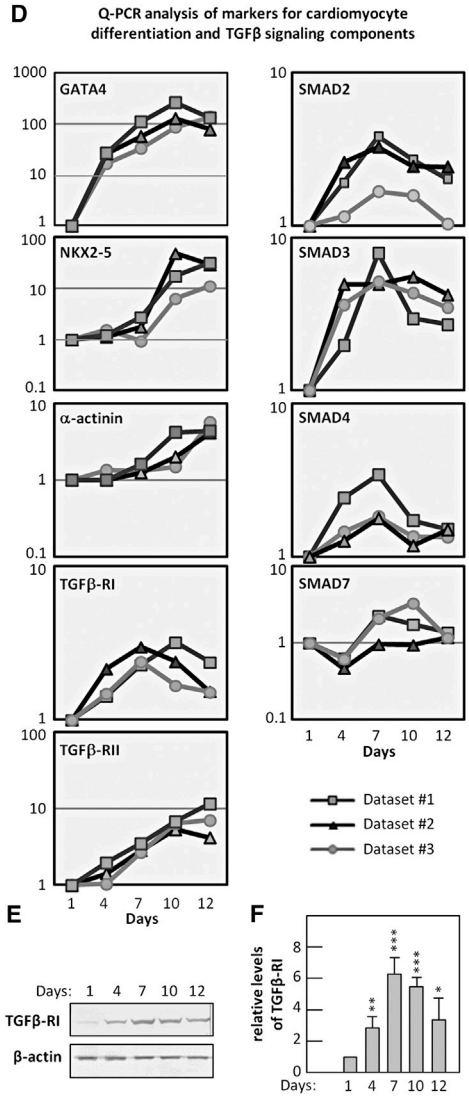

Figure 3. DMSO-Induced P19.CL6 Cell Differentiation into Cardiomyocytes Is Associated with Increased Expression of TGF-β Signaling Components

(A) DIC and IFM of cells during differentiation at days 1 and 14. anti-Sox2, anti-detyrosinated α-tubulin (Glu-tub), anti-GATA4, anti-α-actinin, and DAPI. Bold arrows indicate primary cilia.

(B) Transcriptomics of cell differentiation (days 1–14). Important signaling pathways for cardiomyogenesis and p values are listed (n = 4).

(C) Transcriptomics of differentiating cells relative to day 1. Specific genes and p values are listed (n = 4). Green values indicate gene upregulation. Red values indicate gene downregulation.

(D) Quantitative RT-PCR analysis of differentiation (days 1–12), with relative messenger RNA levels plotted on a log10 scale. Three representative differentiation experiments are presented.

(E) WB of cells (days 1–12) using the indicated antibodies.

(F) Quantification of TGF-β-RI levels relative to day 1 as seen in (E). Shown are means ± SD (n = 5). *p < 0.05; **p < 0.01; ***p < 0.001.

rate of cardiomyogenesis in a bell-shaped and concentration-dependent manner, with 0.2 ng/ml inducing the earliest onset of expression of the markers; at day 2, the level of GATA4 increased ~5-fold compared to cells with DMSO alone (Figures S4A and S4B). Similarly, nuclear GATA4 increased in the presence of TGF-β1 at 0.2 ng/ml, and this was abolished by the TGF-β-RI antagonist SB431542 (Figure S4C). In accordance, TGF-β1 increased the expression of GATA4 and TGF-β-RI, which was inhibited by SB431542 (Figure S4D). Next, cells at day 7 were serum depleted for 24 hr and stimulated with TGF-β1 with and without SB431542. TGF-β1 increased total cellular and CiBa-associated levels of p-SMAD2/3, and this increase was abolished by SB431542 (Figures 4G–4I). Thus, TGF-β signaling stimulates cardiomyogenesis and associates with the CiBa.

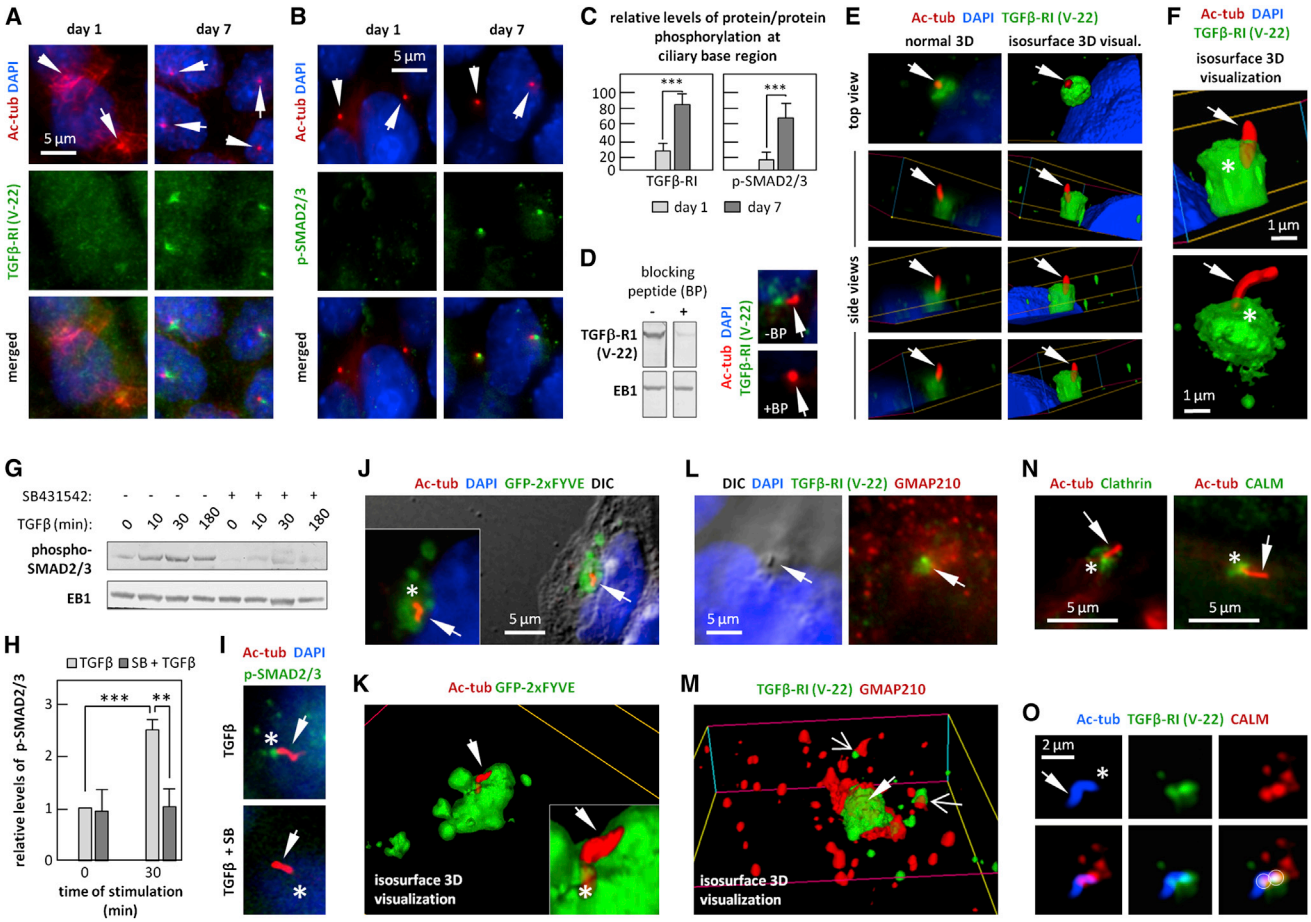

Figure 4. Differentiation of P19.CL6 Cells into Cardiomyocytes Is Associated with Activation of TGF-β Signaling at the CiPo Region

TGF-β1 was used at 0.2 ng/ml.

(A and B) IFM of cells during differentiation at days 1 and 7. Bold arrows indicate primary cilia.

(C) Quantification of TGF-β-RI and p-SMAD2/3 fluorescence levels at the CiBa at days 1 and 7. Shown are means ± SD (n = 32). ***p < 0.001.

(D) WB and IFM of cells at day 7, anti-TGFβ-RI(V-22), and anti-EB1, with and without blocking peptide against anti-TGF-β-RI(V-22). Bold arrows indicate primary cilia.

(E and F) IFM and 3D reconstruction with isosurface visualization of cells at day 7. (E) Normal fluorescence on the acquired stack (left) and isosurface visualization (right). (F) TGF-β-RI(V-22) localization at two different primary cilia in the cell population. Bold arrows indicate primary cilia. Asterisks indicate CiBa.

(G) WB of cells with TGF-β1 for 1, 10, 30, and 180 min with and without SB431542 (2 μM).

(H) Quantification of p-SMAD2/3 levels in SB431542-treated cells compared to untreated cells with TGF-β1 for 30 min as seen in (G). Shown are means ± SD (n = 5). **p < 0.01; ***p < 0.001.

(I) IFM of cells with 0.2 ng/ml TGF-β1 for 30 min with and without SB431542 (2 μM).

(J and K) DIC and IFM (J) and isosurface 3D visualization (K) of cells expressing GFP-2xFYVE (J). Bold arrows indicate primary cilia. Asterisks indicate CiBa.

(L and M) DIC and IFM (L) and isosurface 3D visualization (M) of cells at day 7 of differentiation. Bold arrows indicate primary cilia. Open arrows indicate puncta with colocalization of TGF-β-RI and GMAP210.

(N and O) IFM of cells at day 7 of differentiation. Circles in (O) indicate puncta with strong colocalization of TGF-β-RI and GMAP210. Bold arrows indicate primary cilia. Asterisks indicate CiBa.

We transfected P19.CL6 cells with GFP-2xFYVE, a marker of PI(3)P-containing EEs (Gillooly et al., 2000), and confirmed that the CiPo region is enriched in EEs (Figures 4J and 4K). The Golgi marker (GMAP210) localized around the periphery of the major accumulation of TGF-β-RI at the CiPo, with partial TGF-β-RI colocalization to distinct puncta (Figures 4L and 4M) that may specify Golgi-derived vesicles trafficking TGF-β-Rs to and/or from the CiPo region. Indeed, GMAP210 was shown to anchor IFT20 to the Golgi and regulate sorting or transport of ciliary proteins (Follit et al., 2008). Clathrin and CALM also localized in the CiPo region (Figure 4N) and colocalized with TGF-β-RI (Figure 4O), suggesting that the CiPo of P19.CL6 cells is a site for CDE and internalization of TGF-β-Rs.

DISCUSSION

Primary cilia coordinate many signaling pathways (e.g., Hh and RTK signaling) where ligands bind to their receptors in the ciliary

membrane (Christensen et al., 2012; Goetz and Anderson, 2010) and initiate signal transduction within the ciliary compartment. We found that activation of TGF-β signaling occurs at the CiPo region in fibroblasts and in stem cells differentiating into cardiomyocytes. Here, activation was associated with accumulation of TGF-β-Rs after TGF-β1 stimulation and concomitant increased expression of TGF-β-Rs and downstream signaling components such as SMAD2/3/4 that activate target genes in TGF-β signaling. The CiPo in these cells is a site for CDE, as evidenced by markers for CCP, CCV, and EEs that colocalize with TGF-β-RI. TGF-β signaling through SMAD2/3 at the CiPo was inhibited in hFFs treated with Dynasore and in *Tg737*^{orpk} MEFs with stunted primary cilia, which display reduced CDE. These results directly link TGF-β signaling to the primary cilium, where activation of the pathway may proceed through receptor internalization by CDE at the CiPo.

In fibroblasts, we occasionally observed localization of TGF-β-Rs at the ciliary tip, especially prior to and after prolonged TGF-β stimulation, indicative of intraciliary trafficking of receptors, which we hypothesize are transported after ligand binding to the CiPo for internalization and SMAD2/3 activation. TGF-β-Rs may also initiate signaling within the cilium similar to other receptor types, including PDGFRα, that activate MEK1/2-ERK1/2 in the cilium (Schneider et al., 2005). Alternatively, ligand binding to receptor populations in the plasma membrane in close proximity to the cilium/centrosome axis may be targeted to the CiPo. Targeting and transport of TGF-β-Rs to and within the cilium, as well as termination, recycling, and/or amplification of TGF-β signaling at the cilium, likely involve vesicular trafficking and exocytic and endocytic events that may be regulated by IFT20, Rab GTPases 8/11, and the exocyst complex, which dock at the CiBa and regulate ciliary protein and membrane transport (Das and Guo, 2011; Hsiao et al., 2012). Indeed, TGF-β-Rs were previously shown to be recycled through Rab11-dependent mechanisms (Mitchell et al., 2004), and Rab11 localizes to the CiBa (Hsiao et al., 2012).

Our analysis in MEFs confirms that CDE occurs elsewhere than at the CiPo, as evidenced by formation of CCVs and EEs at the cell periphery in both WT and *Tg737*^{orpk} cells (Figures 2E, 2F, and S2E). However, the CiPo comprises an endocytic compartment that is enriched in CCPs with a 3-fold increase in pits per surface unit at the CiPo membrane compared with the rest of the plasma membrane (Molla-Herman et al., 2010), indicating that a prominent part of CDE-mediated signaling takes place at the cilium. Indeed, the functional output of the TGF-β pathway relies on extensive crosstalk with other signaling pathways, including Hh, Wnt, Notch, mTor, and RTK (Guo and Wang, 2009; Lamouille et al., 2012), which previously were shown to be coordinated by the cilium/centrosome axis. Thus, our findings suggest that the CiBa region offers a unique site for the coordinated crosstalk between TGF-β signaling and other pathways during development and in tissue homeostasis.

Finally, our finding that CDE is disrupted at stunted primary cilia in *Tg737*^{orpk} MEFs may provide knowledge on how defective intraflagellar transport (IFT) leads to aberrant cell signaling coordinated by the primary cilium. Similar to TGF-β signaling, CDE controls the activity of RTK, Hh, and Wnt signaling through the internalization of ligand-bound receptors for either degradation or sustained signaling in endosomes or by recycling of the receptors back to the cell surface (Sorkin and von Zastrow, 2009; McMahon and Boucrot, 2011; Huang and Chen, 2012). In fact, the CiPo region was shown to be a site for both CDE and localization of tumor necrosis factor receptors in fibroblast-like type B synoviocytes (Rattner et al., 2010). Therefore, aberrant signaling observed in *Tg737*^{orpk} MEFs may in part be linked to aberrant CDE activity at the primary cilium, and it will be important to understand how IFT impinges on formation and/or function of the CiPo. Previous studies in trypanosomes showed that IFT mutant cells exhibit major disruptions in organization, orientation, and function of the flagellar pocket (Absalon et al., 2008), which displays remarkable similarity to the CiPo in mammalian cells (Overath and Engstler, 2004). Interestingly, IFT mutants showed major perturbations in vesicular trafficking and reduced endocytosis at the flagellar pocket (Absalon et al., 2008), supporting our finding that IFT88 is associated with regulation of CDE in the CiPo of primary cilia in fibroblasts. Taken together, we suggest that TGF-β signaling is linked to endocytosis at the CiPo and that crosstalk between TGF-β signaling and other signaling pathways is coordinated from this site.

EXPERIMENTAL PROCEDURES

Cell Cultures

Mouse embryonal carcinoma P19.CL6 cells were cultured as described previously (Clement et al., 2009b), and cardiomyocyte differentiation was induced with 1% DMSO (Merck). hFF cells and MEFs were cultured and serum deprived for ciliogenesis (Schneider et al., 2005; Schrøder et al., 2011). hESC (LRB005) were cultured (Laursen et al., 2007; Awan et al., 2010) and induced to differentiate into cardiomyocytes as EBs (Zhang et al., 2009).

Plasmids, Antibodies, and Reagents

GFP-2xFYVE plasmid was a gift from Harald Stenmark (Institute for Cancer Research, Oslo, Norway). Dynasore monohydrate (D7693-5MG) and SB-431542 (S4317) were from Sigma Aldrich, recombinant human TGF-β1 ligand (240-B) was from R&D Systems, DAPI (D1306) was from Molecular Probes, TR-Tf (T2875) was from Life Technologies (T2875), and blocking peptide for TGF-β-RI(V-22) (SC-398P) was from Santa Cruz. See Table S1 for a list of antibodies used.

RNA Isolation

Cells were grown in Petri dishes and were rapidly washed once in ice-cold sterile PBS prior to lysis (1% β-mercaptoethanol) and RNA purification with the NucleoSpin RNA II kit (Macherey-Nagel, 740955-50).

Transcriptome Analysis

Digital gene expression (DGE) tag profiling was performed using an Illumina Genome Analyzer II ('t Hoen et al., 2008). A total of 1 μg RNA per sample was analyzed using Illumina's DGE Tag Profiling Kit according to the manufacturer's protocol (version 2.1B). Tags were filtered and alignment against the mouse genome performed using SOAP (Li et al., 2008), and filtered tags were normalized to 1M tags and functional annotation was performed with DAVID Tools (http://david.abcc.ncifcrf.gov/summary.jsp). Gene set enrichment analysis was performed using the Broad Institute software (http://www.broadinstitute.org/gsea/index.jsp).

Quantitative RT-PCR

Quantitative RT-PCR was performed (Clement et al., 2009a) with the primers listed in Table S2. All samples were run in duplicates and normalized to the

expression of four housekeeping genes: *Gapdh*, *B2m*, *Hprt*, and *Psmd4*. Data were analyzed using the comparative C_t model (Livak and Schmittgen, 2001).

Nucleofection

P19.CL6 cells were transfected by nucleofection with the Nucleofector device II from Amaxa Biosystems (Clement et al., 2009b).

SDS-PAGE and WB Analysis

The analysis was performed as described previously (Christensen et al., 2001). Immunoblots were scanned and processed for publication in Adobe Photoshop CS4 version 11.0. Band intensities were analyzed by densitometric scanning using UN-SCAN-IT 6.1 software (Silk Scientific). For statistical analysis, we used the Student's t test for comparing the variation between two groups. When comparing three or more groups, we used the ANOVA test. All statistical calculations were performed on n = 3 or more. Significance levels were as follows: $^{*}p < 0.05$, $^{**}p < 0.01$, and $^{***}p < 0.001$.

Immunostaining, Microscopy, and Fluorescence Quantification

IFM was done as described previously (Schneider et al., 2005). Images were captured on a fully motorized Olympus BX63 upright microscope with a DP72 color, 12.8-megapixel, 4,140 × 3,096-resolution camera and differential interference contrast (DIC). The software used was Olympus CellSens dimension, which was able to do 3D isosurface projections on captured z stacks, 3D animation videos, and slice views. For quantifications, the mean fluorescence values at the CiBa region were set relative to the fluorescence values in background areas of the cytosol. All statistical calculations were performed with the ANOVA test ($^{**}p < 0.01$; $^{***}p < 0.001$).

ACCESSION NUMBERS

The GEO accession number for the gene expression data reported in this paper is GSE47656.

SUPPLEMENTAL INFORMATION

Supplemental Information includes four figures and two tables and can be found with this article online at http://dx.doi.org/10.1016/j.celrep.2013.05.020.

LICENSING INFORMATION

ACKNOWLEDGMENTS

This work was supported by grants from the Lundbeck Foundation, the Danish Heart Association, the Novo Nordisk Foundation, the Danish Council for Independent Research, Natural Sciences (grants 10-085373 and 09-070398), Nordforsk, the Dagmar Marshalls Foundation, Aase og Ejnar Danielsens Fond, Fonden til Lægevidenskabens Fremme, Arvid Nilssons Foundation, and Reinholdt W Jorck og Hustrus Fond. The Wilhelm Johannsen Centre for Functional Genome Research is established by the Danish National Research Foundation. We thank Prof. Harald Stenmark (Institute for Cancer Research, Norway) for the GFP-2xFYVE plasmid, Lillian Rasmussen and Anni Nielsen for excellent technical assistance, and Prof. Karsten Kristiansen and the Beijing Genomics Institute at Shenzhen for assistance with transcriptomic analysis. S.T.C. and L.A.L. designed and supervised the experiments, and all authors contributed to discussions shaping the investigation. C.A.C. performed the majority of the experiments with the exception of Q-RT-PCR analysis (K.D.A. and C.A.C.), hESC differentiation (M.L.V., C.Y.A.), and data shown in Figure S3 (M.P.R.H.J.). K.K. contributed with differentiation of P19.CL6 cells, and I.R.V. and K.K. performed IFM experiments in fibroblasts. S.T.C. wrote the paper, and all authors read and edited the manuscript.

Received: November 9, 2012
Revised: March 21, 2013
Accepted: May 13, 2013
Published: June 6, 2013

REFERENCES

't Hoen, P.A., Ariyurek, Y., Thygesen, H.H., Vreugdenhil, E., Vossen, R.H., de Menezes, R.X., Boer, J.M., van Ommen, G.J., and den Dunnen, J.T. (2008). Deep sequencing-based expression analysis shows major advances in robustness, resolution and inter-lab portability over five microarray platforms. Nucleic Acids Res. *36*, e141.

Absalon, S., Blisnick, T., Bonhivers, M., Kohl, L., Cayet, N., Toutirais, G., Buisson, J., Robinson, D., and Bastin, P. (2008). Flagellum elongation is required for correct structure, orientation and function of the flagellar pocket in Trypanosoma brucei. J. Cell Sci. *121*, 3704–3716.

Arthur, H.M., and Bamforth, S.D. (2011). TGFβ signaling and congenital heart disease: Insights from mouse studies. Birth Defects Res. A Clin. Mol. Teratol. *91*, 423–434.

Awan, A., Oliveri, R.S., Jensen, P.L., Christensen, S.T., and Andersen, C.Y. (2010). Immunoflourescence and mRNA analysis of human embryonic stem cells (hESCs) grown under feeder-free conditions. Methods Mol. Biol. *584*, 195–210.

Boehlke, C., Kotsis, F., Patel, V., Braeg, S., Voelker, H., Bredt, S., Beyer, T., Janusch, H., Hamann, C., Gödel, M., et al. (2010). Primary cilia regulate mTORC1 activity and cell size through Lkb1. Nat. Cell Biol. *12*, 1115–1122.

Christensen, S.T., Guerra, C., Wada, Y., Valentin, T., Angeletti, R.H., Satir, P., and Hamasaki, T. (2001). A regulatory light chain of ciliary outer arm dynein in Tetrahymena thermophila. J. Biol. Chem. *276*, 20048–20054.

Christensen, S.T., Clement, C.A., Satir, P., and Pedersen, L.B. (2012). Primary cilia and coordination of receptor tyrosine kinase (RTK) signalling. J. Pathol. *226*, 172–184.

Clement, C.A., Larsen, L.A., and Christensen, S.T. (2009b). Using nucleofection of siRNA constructs for knockdown of primary cilia in P19.CL6 cancer stem cell differentiation into cardiomyocytes. Methods Cell Biol. *94*, 181–197.

Clement, C.A., Kristensen, S.G., Møllgård, K., Pazour, G.J., Yoder, B.K., Larsen, L.A., and Christensen, S.T. (2009a). The primary cilium coordinates early cardiogenesis and hedgehog signaling in cardiomyocyte differentiation. J. Cell Sci. *122*, 3070–3082.

Corbit, K.C., Shyer, A.E., Dowdle, W.E., Gaulden, J., Singla, V., Chen, M.H., Chuang, P.T., and Reiter, J.F. (2008). Kif3a constrains beta-catenin-dependent Wnt signalling through dual ciliary and non-ciliary mechanisms. Nat. Cell Biol. *10*, 70–76.

Das, A., and Guo, W. (2011). Rabs and the exocyst in ciliogenesis, tubulogenesis and beyond. Trends Cell Biol. *21*, 383–386.

Egorova, A.D., Khedoe, P.P., Goumans, M.J., Yoder, B.K., Nauli, S.M., ten Dijke, P., Poelmann, R.E., and Hierck, B.P. (2011). Lack of primary cilia primes shear-induced endothelial-to-mesenchymal transition. Circ. Res. *108*, 1093–1101.

Ezratty, E.J., Stokes, N., Chai, S., Shah, A.S., Williams, S.E., and Fuchs, E. (2011). A role for the primary cilium in Notch signaling and epidermal differentiation during skin development. Cell *145*, 1129–1141.

Follit, J.A., San Agustin, J.T., Xu, F., Jonassen, J.A., Samtani, R., Lo, C.W., and Pazour, G.J. (2008). The Golgin GMAP210/TRIP11 anchors IFT20 to the Golgi complex. PLoS Genet. *4*, e1000315.

Ghossoub, R., Molla-Herman, A., Bastin, P., and Benmerah, A. (2011). The ciliary pocket: a once-forgotten membrane domain at the base of cilia. Biol. Cell *103*, 131–144.

Gillooly, D.J., Morrow, I.C., Lindsay, M., Gould, R., Bryant, N.J., Gaullier, J.M., Parton, R.G., and Stenmark, H. (2000). Localization of phosphatidylinositol 3-phosphate in yeast and mammalian cells. EMBO J. *19*, 4577–4588.

Goetz, S.C., and Anderson, K.V. (2010). The primary cilium: a signalling centre during vertebrate development. Nat. Rev. Genet. *11*, 331–344.

Guo, X., and Wang, X.F. (2009). Signaling cross-talk between TGF-beta/BMP and other pathways. Cell Res. *19*, 71–88.

Habara-Ohkubo, A. (1996). Differentiation of beating cardiac muscle cells from a derivative of P19 embryonal carcinoma cells. Cell Struct. Funct. *21*, 101–110.

Hildebrandt, F., Benzing, T., and Katsanis, N. (2011). Ciliopathies. N. Engl. J. Med. *364*, 1533–1543.

Hsiao, Y.C., Tuz, K., and Ferland, R.J. (2012). Trafficking in and to the primary cilium. Cilia *1*, 4.

Huang, F., and Chen, Y.G. (2012). Regulation of TGF-b receptor activity. Cell and Bioscience *2*.

Kirchhausen, T., Macia, E., and Pelish, H.E. (2008). Use of dynasore, the small molecule inhibitor of dynamin, in the regulation of endocytosis. Methods Enzymol. *438*, 77–93.

Lamouille, S., Connolly, E., Smyth, J.W., Akhurst, R.J., and Derynck, R. (2012). TGF-β-induced activation of mTOR complex 2 drives epithelial-mesenchymal transition and cell invasion. J. Cell Sci. *125*, 1259–1273.

Laursen, S.B., Møllgård, K., Olesen, C., Oliveri, R.S., Brøchner, C.B., Byskov, A.G., Andersen, A.N., Høyer, P.E., Tommerup, N., and Yding Andersen, C. (2007). Regional differences in expression of specific markers for human embryonic stem cells. Reprod. Biomed. Online *15*, 89–98.

Li, R., Li, Y., Kristiansen, K., and Wang, J. (2008). SOAP: short oligonucleotide alignment program. Bioinformatics *24*, 713–714.

Lienkamp, S., Ganner, A., and Walz, G. (2012). Inversin, Wnt signaling and primary cilia. Differentiation *83*, S49–S55.

Livak, K.J., and Schmittgen, T.D. (2001). Analysis of relative gene expression data using real-time quantitative PCR and the 2(-Delta Delta C(T)) method. Methods *25*, 402–408.

McMahon, H.T., and Boucrot, E. (2011). Molecular mechanism and physiological functions of clathrin-mediated endocytosis. Nat. Rev. Mol. Cell Biol. *12*, 517–533.

Mitchell, H., Choudhury, A., Pagano, R.E., and Leof, E.B. (2004). Ligand-dependent and -independent transforming growth factor-beta receptor recycling regulated by clathrin-mediated endocytosis and Rab11. Mol. Biol. Cell *15*, 4166–4178.

Molla-Herman, A., Ghossoub, R., Blisnick, T., Meunier, A., Serres, C., Silbermann, F., Emmerson, C., Romeo, K., Bourdoncle, P., Schmitt, A., et al. (2010). The ciliary pocket: an endocytic membrane domain at the base of primary and motile cilia. J. Cell Sci. *123*, 1785–1795.

Overath, P., and Engstler, M. (2004). Endocytosis, membrane recycling and sorting of GPI-anchored proteins: Trypanosoma brucei as a model system. Mol. Microbiol. *53*, 735–744.

Poole, C.A., Flint, M.H., and Beaumont, B.W. (1985). Analysis of the morphology and function of primary cilia in connective tissues: a cellular cybernetic probe? Cell Motil. *5*, 175–193.

Rattner, J.B., Sciore, P., Ou, Y., van der Hoorn, F.A., and Lo, I.K. (2010). Primary cilia in fibroblast-like type B synoviocytes lie within a cilium pit: a site of endocytosis. Histol. Histopathol. *25*, 865–875.

Satir, P., Pedersen, L.B., and Christensen, S.T. (2010). The primary cilium at a glance. J. Cell Sci. *123*, 499–503.

Schneider, L., Clement, C.A., Teilmann, S.C., Pazour, G.J., Hoffmann, E.K., Satir, P., and Christensen, S.T. (2005). PDGFRalphaalpha signaling is regulated through the primary cilium in fibroblasts. Curr. Biol. *15*, 1861–1866.

Schrøder, J.M., Larsen, J., Komarova, Y., Akhmanova, A., Thorsteinsson, R.I., Grigoriev, I., Manguso, R., Christensen, S.T., Pedersen, S.F., Geimer, S., and Pedersen, L.B. (2011). EB1 and EB3 promote cilia biogenesis by several centrosome-related mechanisms. J. Cell Sci. *124*, 2539–2551.

Sorkin, A., and von Zastrow, M. (2009). Endocytosis and signalling: intertwining molecular networks. Nat. Rev. Mol. Cell Biol. *10*, 609–622.

Tang, W.B., Ling, G.H., Sun, L., and Liu, F.Y. (2010). Smad anchor for receptor activation (SARA) in TGF-beta signaling. Front Biosci. (Elite. Ed.) *2*, 857–860.

Waters, A.M., and Beales, P.L. (2011). Ciliopathies: an expanding disease spectrum. Pediatr. Nephrol. *26*, 1039–1056.

Zhang, J., Wilson, G.F., Soerens, A.G., Koonce, C.H., Yu, J., Palecek, S.P., Thomson, J.A., and Kamp, T.J. (2009). Functional cardiomyocytes derived from human induced pluripotent stem cells. Circ. Res. *104*, e30–e41.